WIND TUNNEL TESTING OF LOW-DRAG AIRFOILS

W. D. Harvey, R. J. McGhee, and C. D. Harris
NASA Langley Research Center
Hampton, Virginia 23665

ABSTRACT

Results are presented for the measured performance recently obtained on several airfoil concepts designed to achieve low drag by maintaining extensive regions of laminar flow without compromising high-lift performance. The wind tunnel results extend from subsonic to transonic speeds and include boundary-layer control through shaping and suction. The research was conducted in the NASA Langley 8-Ft. Transonic Pressure Tunnel (TPT) and Low Turbulence Pressure Tunnel (LTPT) which have been developed for testing such low-drag airfoils. Emphasis is placed on identifying some of the major factors influencing the anticipated performance of low-drag airfoils.

INTRODUCTION

Application of laminar flow concepts to aircraft design depends on fabrication, materials, and ease of maintaining laminar flow. The benefits of laminar flow are measured by achievement of very low drag which depends on the total wetted surface that is maintained laminar under various flight conditions. Performance at off-design conditions and surface maintenance tolerances are also of importance. Successful laminar flow application may cause significant changes in the trend of future aircraft design.

Whereas wing loadings on recent aircraft designs have been increasing, a laminar flow airplane will generally have a lower wing loading than a turbulent one. This effect occurs because of the type of pressure distribution required to yield the insensitivity to surface conditions and provides for long runs of laminar flow. Large laminar flow airplanes (transports) will almost surely operate at high altitudes to minimize Reynolds number effects and thus maximize performance.

Considerable basic research and technology, with and without boundary-layer control, is available (refs. 1-12) and believed suitable for design and construction of an aircraft wing to achieve laminar flow with reasonable success at subsonic speeds. Interest in this capability has been renewed by the inflight and wind tunnel test results obtained on several aircraft to establish the existence of natural laminar flow (NLF) on recent production-quality general-aviation airframe surfaces in typical operating environments (refs. 13-15). These results were based primarily on flow visualization (sublimating chemicals) techniques to define transition location and provide increased knowledge and understanding for present day aircraft. However, many of the wings investigated incorporated turbulent airfoil sections and were not designed to achieve laminar flow.

Laminarization has proven to be an inherently difficult boundary-layer stability problem to analyze and control due to influences of various local and external disturbances. This difficulty becomes more acute when sweep effects are included at high speeds. For this reason, a good understanding of the various stability theories along with advanced design technology will be required for the development and certification of future high performance aircraft with laminar flow aerodynamics. The emergence of advanced design codes, boundary-layer stability analysis methods, composite materials, and new fabrication technology can substantially alleviate previous laminarization concerns and encourage aerodynamicists to design better airfoils with higher lift-to-drag ratios. The Airfoil Aerodynamics Branch at Langley Research Center is currently involved in utilizing these emerging technologies to develop low-drag airfoils over a wide range of conditions. One such effort is directed toward developing natural laminar flow (NLF) airfoils for general-aviation applications which combine the high maximum lift capability of new NASA high-lift airfoils (refs. 16-18) with the low-drag characteristics of the NACA 6-series airfoils. A major design goal of these airfoils is to avoid degradation of high-lift performance characteristics if the flow becomes fully turbulent. Another effort is directed toward research on large-scale swept laminar flow control (LFC) airfoils at transonic speeds to evaluate the compatibility of suction laminarization and supercritical technology at conditions which are typical of high-performance transport aircraft (refs. 6, 19).

The purpose of this paper is to develop a better understanding of the wind tunnel testing environment and its influences on the measured performance of several advanced low-drag airfoil concepts designed to achieve extensive regions of laminar flow. The wind tunnel results extend from subsonic to transonic speeds and include boundary-layer control. The low-speed research was conducted in the Langley Low Turbulence Pressure Tunnel (LTPT), and the transonic research was conducted in the NASA Langley 8-Ft. Transonic Pressure Tunnel. These tunnels were developed or modified for testing low-drag airfoils.

SYMBOLS

c	airfoil chord
c_d	section profile-drag coefficient
c_ℓ	section lift coefficient
c_m	section pitching-moment coefficient at quarter-chord
C_p	pressure coefficient, $(p-p_\infty)/q_\infty$
C_p^*	pressure coefficient for local sonic velocity

C_Q	suction coefficient
h	height
L/D	lift-to-drag-ratio, c_ℓ/c_d
M_∞	free-stream Mach number
p	static pressure
$\tilde{p}$	rms pressure fluctuation
q	dynamic pressure
R	unit Reynolds number
R_c	Reynolds number based on chord
$(R_x)_{tr}$	Reynolds number based on transition location
t	section maximum thickness
u,v	velocity
$\tilde{u}$	rms velocity fluctuations
x,y	chordwise and spanwise coordinate system
α	angle of attack
δ_f	flap deflection angle, degrees
Λ	leading-edge sweep, degrees
λ	wavelength

Subscripts:

B	balance
c	corrected
max	maximum
s	suction
tot	total
tr	transition
w	wake
∞	free-stream conditions

LOW-DRAG CHARACTERISTICS

The drag due to friction on a current transport aircraft at cruise conditions with turbulent boundary layers is approximately 60% of the total drag. Induced drag accounts for most of the balance. The friction drag approaches nearly 90% of the total drag for submersible vehicles. It is clear, then, that there is room for performance improvements in either case by reducing the drag.

In principle, the most promising approach towards achieving significant drag reduction is through the stabilization and maintenance of the laminar boundary layer as long as possible such that most of the friction drag remains at the laminar rather than the turbulent level. It is expected (ref. 20) that techniques involving local flow manipulators may soon be available for reduction of the turbulent friction drag of regions of the aircraft that are not laminarized. However, such techniques are not anticipated to give drag reduction levels comparable to that of maintaining laminar flow. These techniques will not be discussed herein and only pre-transition concepts are considered.

Past and present wind tunnel research and development and wing-glove flight testing have established pressure and friction as the two major sources of aerodynamic drag. The most effective approach of reducing drag is by geometric shaping (passive) and minimization of wetted area (active), respectively. These approaches have provided a means of maintaining laminar flow over extensive lengths with subsequent low drag.

Passive Method - Geometric Shaping Control

The passive or natural laminar flow (NLF) approach involves stabilizing laminar boundary layers by producing a favorable pressure gradient through geometric shaping and requires no active system for control. The exploitation of favorable pressure gradient can be traced back to the development of the NACA 6-series airfoils and sailplane airfoils as well as more recent airfoils developed by Somers (ref. 16) and Viken (ref. 17).

If flow can be maintained laminar over the entire favorable pressure gradient region, it will either undergo transition just beyond the pressure minimum or else proceed to laminar separation with subsequent transition to turbulent flow. Which of these flow processes occurs will depend on several factors that include the geometric shape, angle of attack, local Reynolds number, and surface conditions. These combined factors can also produce a hysteresis effect in the lift performance that is often observed for low Reynolds number airfoils (ref. 21). Thus the major objective is to shape the airfoil contour to have as extensive a region of favorable pressure gradient as possible to ensure laminar flow followed by an appropriate recovery in the adverse pressure gradient region for maintaining attached flow. This becomes more difficult to accomplish the more rearward the favorable pressure gradient is retained. As one approaches transonic speeds, shaping becomes more important in order to minimize pressure peaks in the nose region and

shock formation in the rear adverse pressure gradient (ref. 22). In addition, inherent instabilities due to boundary-layer crossflow at the leading edge of swept wings and in the rear pressure rise regions become very difficult to control passively (refs. 5-8, 23-24).

Active Method - Suction Control

A detailed discussion and summary review of a large number of suction control (LFC) investigations, including both wind tunnels and flight results, have been presented by Pfenninger (ref. 5). In general, large reductions in friction and profile drag were achieved with LFC as compared with turbulent flow.

Active approaches usually depend on both shaping and mass transfer through local suction or blowing concepts. This concept appears to be the most attractive way of laminarization for low drag, especially when sweep is required at the higher speeds. Flight experience has shown that on swept wings the transition location is considerably further forward than on unswept wings as reported earlier (refs. 7-10) and recently by Holmes et al. (ref. 13). Earlier transition on swept wings is probably caused by unstable boundary-layer profiles in the direction normal to the potential streamlines that create a crossflow in the immediate leading-edge region and rear pressure rise regions (refs. 6, 23-24). These crossflow instabilities are less responsive to suction control than Tollmien-Schlichting instabilities which develop in the streamwise direction or constant pressure regions. Weakly amplified oblique Tollmien-Schlichting waves can superimpose on crossflow disturbances causing distortion of the crossflow vortices that are stretched and converged downstream. The resulting nonlinear interaction of different disturbance modes will cause the less stable crossflow vortices to grow considerably faster than predicted by linearized stability theory. It is anticipated that this interaction can be minimized by designing swept low-drag wings so that crossflow is only critical over a small percentage of the chord. In the nose region, this may be accomplished by reducing both the sweep angle and nose radius to acceptable design values. In the aft region, control of adverse pressure gradient should be the objective.

The boundary-layer development and stability limits of these crossflow profiles, as well as the Tollmien-Schlichting instabilities, and the boundary-layer air which must be removed to stabilize either can be calculated by numerous available theories (refs. 6, 23-27). However, these methods require arbitrary choice of the growth limitation of the disturbances or transition location as input to the theory. Thus, these methods should serve only as a guide in the design process.

Because one of the key elements to the successful achievement of very low drag with or without boundary-layer control is the question of surface tolerance, it is important to recognize that no easing of tolerances is afforded by boundary-layer suction or shaping if both the speed and unit Reynolds number increase (refs. 5, 7, 8, 14, 28, 29). In

attainment of low drag by NLF, success depends on surface shape and ability to control smoothness. Similarly, for suction surfaces, the boundary-layer stability Reynolds number is held to below limiting values by keeping the boundary layer thin. However, thin boundary layers are inherently developed by increasing Reynolds number and suction and require surfaces with correspondingly smaller roughness and waviness (refs. 5-6, 19).

The turbulent boundary-layer flow over the fuselage of an aircraft can spread from the wing juncture along the attachment line causing contamination. This effect will increase with sweep. Such leading-edge contamination can be avoided by keeping the critical momentum thickness Reynolds number below 100 (ref. 30). This may be accomplished by applying a fence for shielding the inboard turbulent boundary layer from spreading, or reducing sweep angle and leading-edge radius (ref. 5).

Steep pressure gradients due to shock waves can cause separation of the boundary layer and substantial increases in drag. Earlier efforts (ref. 5) and recent in-house analysis and tests (ref. 19) suggest that suction laminarization appears basically feasible in regions of weak shocks at transonic conditions. Apparently, the pressure rise which a laminar boundary layer with suction can sustain in regions of shock interaction decreases with length Reynolds number, unless the upstream boundary-layer thickness is reduced by appropriate suction (ref. 31). In summary, the above discussed effects (sweep, disturbances, contamination, shocks, etc.) impose design challenges to maintaining extensive laminar flow and low drag.

LAMINARIZATION ASPECTS

Some of the major factors known to affect transition on low-drag airfoils are surface roughness, waviness, pressure gradient, Reynolds number, suction-induced disturbances, crossflow instability, and wind tunnel or flight environment. A prerequisite for laminarization is a surface finish compatible with the boundary-layer thickness for which the investigation is undertaken. Three-dimensional surface-induced disturbances become primary sources for distortion of growth disturbances in the absence of sweep-induced crossflow effects. However, in comparison with small scale experiments in low turbulence wind tunnels, somewhat increased two- and three-dimensional surface roughness seems permissible in flight (refs. 5, 7, 8, 14, 28, 29). Thus, conclusions from low-drag experiments in wind tunnels often result in misleading and/or unduly pessimistic views about surface roughness or waviness requirements.

Wind tunnel turbulence and noise influence the transition process, and the isolation of these effects requires the total elimination or control of the other known factors (refs. 32-34). The objective of achieving very low wind tunnel disturbance levels approaching anticipated flight simulation levels becomes increasingly difficult as one moves from subsonic to transonic speeds or increases Reynolds number at a given

speed. The characteristic disturbances increase in proportion to the tunnel speed or pressure level. Thus, the ability to simulate a free air environment diminishes with the existence and increased level of stream turbulence, radiated sound from the wall boundary layer or drive system, diffuser flow separation disturbances, mechanical vibrations, etc. Previous investigations in wind tunnels and flight have clearly shown that the maximum transition Reynolds numbers obtained with and without suction (ref. 19) on simple and complex geometries critically depend on the characteristic disturbance level and broadband frequency present. Figure 1 summarizes a large quantity of experimental data from previous investigations (refs. 19, 34) that show the effect of disturbance level on transition Reynolds number. The data indicate that low disturbance levels are required ($\tilde{u}/u \ll 0.1\%$) for maximum transition Reynolds numbers in wind tunnels. However, there may be limitations in the ability of facilities to achieve diminished disturbance levels and scales compared with flight.

Laminarizing the flow on subscale airfoil models in wind tunnels is generally a more difficult aerodynamic problem than on full scale wing surfaces in flight as previously discussed. In particular, the achievement of moderately high chord Reynolds number simulation on practical size models in most wind tunnels requires testing at high unit Reynolds numbers where characteristic tunnel disturbances dominate, causing early transition. Laminar separation without reattachment may occur at very low Reynolds numbers causing difficulty in measuring airfoil performance (ref. 21). Wind tunnel testing at high unit Reynolds numbers adversely influences the surface tolerance critieria for both NLF and LFC and will strongly affect the suction surface and metering system design; physical dimensions are frequently so small that practical fabrication tolerances for certain model features become difficult to accomplish (refs. 6, 19). Thus, wind tunnel selection is very important for low-drag testing. The major objective is to be able to test large chord and aspect ratio models to reduce scale effects and to have good flow quality.

Establishing the lift performance of low-drag or even turbulent airfoils is very important. Lift performance can be influenced in wind tunnels by large adverse pressure gradients induced by the airfoil at high angles of attack which can cause sidewall juncture boundary-layer separation. Obviously, this separated flow can influence the pressure distribution on the wing and spread across the airfoil span, causing both loss of laminar flow and lift performance. This influence can be compounded by the addition of leading- and trailing-edge high-lift devices on the airfoil during wind tunnel testing. Thus, consideration must be given to model aspect ratio and to sidewall boundary-layer control for high-lift testing.

FACILITIES FOR LOW-DRAG TESTING

Low-Turbulence Pressure Tunnel (LTPT)

The Langley Low-Turbulence Pressure Tunnel (LTPT) is a single-return closed-circuit tunnel which can be operated at pressures from near-vacuum to 10 atmospheres. The test section is rectangular in shape (3 feet wide and 7.5 feet in height and length) and the contraction ratio is 17.6:1. The LTPT is capable of testing at Mach numbers from 0.05 to 0.50 and unit Reynolds numbers from 0.1×10^6 to 15×10^6 per foot. This tunnel has provisions for removal of the sidewall boundary layer by means of a closed-loop suction system mounted inside the pressure chamber. This system utilizes slotted vertical sidewalls just ahead of the model test section, and the removed air is reinjected through an annular slot downstream of the test section. A flow control system allows the flow and pressure requirements to be varied as dictated by tunnel operation. This system can be used to provide boundary-layer control (BLC) for airfoil research.

A BLC system for high-lift airfoil testing is also available. This system utilizes compressed dry air and involves tangential blowing from slots located on the sidewall mounting endplates. Flowmeters can be used to monitor the amount of air blown into the tunnel. An automatically controlled vent valve is utilized to remove the air injected into the tunnel by this system. A high-lift model support and force balance system is provided to handle both single-element and multiple-element airfoils.

The measured turbulence level of the LTPT is very low due to the large contraction ratio and the nine fine-mesh antiturbulence screens. This excellent flow quality facility is particularly suitable for testing low-drag airfoils. Recent flow quality measurements in the LTPT indicate that the velocity fluctuations in the test section range from 0.025 percent at Mach 0.05 to 0.30 percent at Mach 0.20 at the highest unit Reynolds number (refs. 35, 36).

The drive system is a 2000-horsepower direct-current motor with power supplied from a motor-generator set. The tunnel stagnation temperature is controlled by a heat exchanger which provides both heating and cooling using steam injectors and modulated valves that control the flow volume of water through a set of coils. A complete description and calibration of the tunnel are reported in reference 37.

8-Ft. Transonic Pressure Tunnel (8-Ft. TPT)

The Langley 8-Foot Transonic Pressure Tunnel is a closed-circuit single-return variable density continuous-flow wind tunnel with a contraction ratio of 20:1. The test section walls are slotted (5 percent porosity) top and bottom, with solid sidewalls fitted with windows for schlieren flow visualization. In 1981 the facility was modified for flow quality improvements and reconfigured for low-drag testing of a

large-chord swept laminar-flow-control airfoil at transonic speeds (ref. 19). A honeycomb and five screens were permanently installed in the settling chamber to suppress the turbulence level in the test section. A contoured liner was installed on all four walls of the test section to simulate interference-free flow about an infinite yawed wing. This contoured liner produces a contraction ratio of 25:1 and covers existing floor and ceiling slots. An adjustable sonic throat is also located at the end of the test section to block upstream propagation of diffuser noise.

The combination of honeycomb, screens, and choke provides a very low disturbance level ($\tilde{p}/p \approx 0.05\%$) in the test region at transonic speeds. Except for the honeycomb and screens, the modifications are reversible. In the current configuration, the stagnation pressure can be varied from about 0.25 to 1.25 atmospheres up to a Mach number of less than 0.85 with the transonic slots closed by the liner. The stagnation temperature is controlled by a water-cooled radiator upstream of the settling chamber. Tunnel air can be dried by a dryer using silica gel desiccant to prevent fogging due to expansion in the high-speed nozzle.

RESULTS AND DISCUSSION

Past and present wind tunnel and in-flight testing has shown that the maintenance of extensive regions of laminar flow by the use of NLF or LFC approaches can provide significant drag reduction for improved aircraft performance. The following discussion is a review of recent wind tunnel tests of advanced design concepts (refs. 17, 19, 38) for low-drag airfoils and some of the effects that the wind tunnel environment has on those results. Also, it is intended to identify influences that are known to affect performance results obtained in wind tunnels that, if not taken into account, can cause concern and rejection of such low-drag airfoils for future application. Several of the 2-D/3-D designed airfoil configurations (refs. 17, 38, 39) shown herein were discussed in detail earlier in this workshop along with discussions of integrated trailing-edge flap designs (ref. 40) for the medium- to high-speed NLF airfoil designs. Thus, no detailed discussion of design concepts will be presented here, only background information, experimental verification, and factors that influence overall results.

Tunnel Flow Quality

Aside from other factors known to affect transition on low-drag airfoils, the maximum transition Reynolds number, with or without boundary-layer control, critically depends on the characteristic disturbance level and broadband frequencies generated in wind tunnels utilized for testing (fig. 1). An example of this effect is shown in figure 2 for several airfoils recently tested in the two NASA Langley wind tunnels developed and used for low drag research. Both facilities operate above and below atmospheric pressure, providing a wide range of Reynolds

numbers and Mach numbers from $0.05 < M_\infty < 0.85$ as currently configured. The present flow quality values were measured with conventional hot-wire and acoustic probe techniques (ref. 33). Transition location on the airfoils was measured using surface thin film gages (ref. 41) and is a routine requirement for assessment of laminar patterns or state of the local boundary layer.

For either the NLF or LFC airfoil results in figure 2, the measured logarithm of transition-length Reynolds number varies inversely in proportion to the logarithm of the tunnel disturbance level. As expected, the indicated levels for $(R_x)_{tr}$ with LFC applications are significantly higher than those without suction control as can be seen by comparing past (ref. 12) and present results obtained in the LTPT ($M \approx 0.20$). It should be noted that the extensive lengths of laminar flow measured on the new NASA airfoils (figure 2) generally agree with expectations and that this achievement may in part be attributed to excellent flow quality. Thus, the achievement of high transition Reynolds numbers for low-drag testing may not be possible if acceptable flow quality cannot be realized in test facilities. The selection of suitable facilities would, of course, imply the need for measured and documented flow quality for assessment.

Low-Speed Airfoils - Surface Tolerances

Figure 3 illustrates the airfoil shape and near design velocity distribution over both surfaces and represents a concept developed by industry for long endurance operation requiring high L/D. This configuration was shaped to provide a velocity profile or favorable pressure gradient suitable for maintaining laminar flow back to $x/c \approx 0.30$ on the upper and $x/c \approx 0.75$ on the lower surfaces at a chord Reynolds number of 14×10^6 with zero sweep. This geometry type and velocity distribution are not entirely unfamiliar to today's aerodynamicists in that they resemble those which may be found on sailplanes, low-speed aircraft, and business jets that have utilized NLF for drag reduction and improved performances.

A model of the long endurance airfoil concept was constructed of metal with a 2.7 foot chord and aspect ratio near 1 and instrumented with pressure orifices. The photograph in figure 4 shows the model removed from the tunnel and is a view of the underside leading-edge region illustrating the removable metal cover plate located at near mid-span for access to internal instrumentation and leads. The model was initially tested as received with only minor cleaning of the surface with diluted alcohol.

Wake-rake drag measurements were obtained in the LTPT at one model chord length downstream of the trailing edge at spanwise stations of $y/c = 0$ (mid-span) and $y/c = 0.325$ (10.4 inches from mid-span). The measured surface pressures were integrated to obtain airfoil section lift coefficients. Performance of the low endurance airfoil is summarized in figure 5 for $M_\infty = 0.1$ and $R_c = 14 \times 10^6$ with and without fixed transition. The results clearly indicate that the drag levels obtained

at mid-span (y/c = 0.0) with free transition were extremely high, indicative of only small lengths of laminar flow. This result is supported by a comparison of the drag levels obtained at mid-span with free or fixed transition on the upper and lower surfaces at x = 0.03c.

Visual inspection of the model prior to this initial test revealed that the lower surface may have had adverse roughness effects due to the model cover plate. Therefore, the model was sanded on both surfaces with number 600 carborundum paper and thoroughly cleaned with diluted alcohol in an effort to eliminate the suspected cause for loss of laminar flow. Further precaution was taken by also lightly wiping the surface with a special cloth (tack rag) to remove lint and dust settlement on the horizontally mounted model. Drag measurements were then made at the spanwise station y/c = 0.325 to minimize possible lower-surface cover-plate disturbance effects. Figure 5 shows that a drag coefficient of about 0.0055 was measured at a lift coefficient of about 1.2 (L/D ≈ 218), signifying a large gain in the extent of laminar flow for the improved surface conditions. Upon completion of the test, surface waviness measurements were made at both spanwise stations using a surface dial indicator with fixed legs on a solid base spaced 2 inches apart. The resolution of the dial indicator was determined to be 0.0005 inches. The measured waviness on the long endurance airfoil indicated possible excessive waviness at the mid-span station on both surfaces that would be unacceptable for wind tunnel models and low-drag tests. For example, several waves with height-to-wavelength ratio of $h/\lambda = 0.003$ were measured on both surfaces near x/c = 0.15.

Previous research by Carmichael (refs. 28, 29) on low-drag airfoils with and without sweep has provided an empirical expression that represents local allowable waviness for single waves. Carmichael further suggested that one could estimate tolerances for closely spaced multiple waves by multiplying the single wave expression by a factor of 1/3. Since multiple waves were present on the long endurance model surface, the measured $h/\lambda = 0.003$ for single waves was reduced by this factor and compared to Carmichael's empirical expression for several Reynolds numbers and constant sweep angle of 30° (figure 6). Carmichael has shown that only a small reduction in allowable multiple waviness exists for a swept wing compared to unswept wings at low speeds. Also, included in figure 6 are measured values of allowable waviness obtained for other low-drag airfoil models tested in the NASA Langley 8-Ft. TPT and LTPT and subsequently discussed herein. The present results clearly indicate the need for tight control of fabrication tolerances on low-drag wind tunnel models due to scale effects. These tolerances, however, may be relaxed for full scale aircraft surfaces, as suggested in a recent review by Holmes et al. (ref. 14), since scale effects are greatly reduced both by wing chord and low unit Reynolds numbers at cruise conditions ($R/ft < 2 \times 10^6$). The extent of laminar flow at mid-span on the long endurance airfoil model at $R_c = 14 \times 10^6$ ($R/ft = 5.2 \times 10^6$) was probably influenced by increased tunnel turbulence level associated with high unit Reynolds number, in addition to sensitivity of surface conditions.

Recent experimental performance results have been obtained in the LTPT for a low-speed NLF airfoil (ref. 18), designated NLF(1)-0414F, and details of the design features are given by Viken (ref. 38). In general, the design objective for this airfoil was to obtain very low cruise drag coefficients by selective shaping of the contour to provide a favorable pressure gradient with extensive laminar flow regions over both upper and lower surfaces and high maximum lift. The design conditions were $c_\ell = 0.43$, $R_c = 10 \times 10^6$, $M_\infty < 0.40$, and thickness ratio of $t/c = 0.14$. Figure 7 illustrates the calculated design pressure distribution and airfoil section shape. A simple trailing-edge flap having a length equal to 0.125c was incorporated to substantially increase the low-drag c_ℓ range. As can be seen from the design favorable pressure gradient (figure 7), laminar flow is anticipated over both upper and lower surfaces rearward to $x/c = 0.70$. Furthermore, design considerations were given to the achievement of gentle stall characteristics and to maintaining an acceptable lift performance if the airfoil becomes turbulent.

Representative airfoil section data obtained with wake rake and surface pressures are presented in figure 8 for the design Reynolds number with and without fixed transition in the indicated nose regions. For the free transition case, laminar flow was measured on both surfaces back to $x/c = 0.70$ and will be subsequently shown and discussed. Figure 8 shows that a minimum drag coefficient of about 0.0027 was measured at the design lift of about 0.40. This corresponds to $L/D \approx 160$ with zero flap deflection. Furthermore, a value of 1.8 for the maximum lift coefficient was obtained at an angle of attack of 18° while the pitching moment remained relatively constant. However, of major significance is the fact that fixing transition near the leading edge had only a very small effect on the lift performance and $(c_\ell)_{max}$ value at the expense of drag increase. This finding is believed to be a very important improvement over the previous NACA 6-series airfoils which have adverse stall characteristics. In other words, this new NLF airfoil design can also be classified as a very good turbulent flow airfoil in terms of lift performance as well as drag level and pitching moment.

Transition location on the airfoil upper surface was determined by using small thin-film gages that were glued to the model surface at several chordwise and spanwise locations and spaced to eliminate interference effects from one another. These instruments basically operate on the same principle as hot-wire anemometry with overheat ratio set for the sensitivity required for the detection of the state of the local boundary layer where they are placed (ref. 41). This is accomplished by utilizing characteristic behavior of the gages for detection of local changes in heating due to shear stresses of either a laminar, transitional, or turbulent boundary layer. These local changes are recorded as variation of rms output signals with time and require a sufficient number of these gages to be spatially located on the surface to properly identify patterns.

It is essential that each thin-film gage experience a known laminar, transitional, and turbulent flow output signal for a given investigation in order to reference and properly interpret results. This may either be accomplished by starting at sufficiently low Reynolds number test conditions where the output signals for all gages are known to be laminar or by locating a reference gage where it always senses a known turbulent or laminar boundary layer for comparison. Caution should be used when these conventional type gages are located in separated flow zones as to interpretation of results. The output signals in such a zone may indicate similar signals to those for turbulent attached flow.

Figure 9 shows example results taken by J. P. Stack (NASA Langley) from surface mounted thin-film gages on an NLF airfoil model in the LTPT. The gage located at $x/c = 0.40$ and in a known laminar flow region indicates a time-dependent low-level rms output signal with essentially no deviations above or below the mean. As the laminar boundary layer approaches its stability limit, laminar-to-turbulent bursts are locally detected with elapsed time as indicated for $x/c = 0.5$ location. The flow becomes progressively unstable downstream (or with increased Reynolds number) until peak transition occurs with a higher rms level and very random signal with time as seen for $x/c = 0.6$. Once the flow goes through transition to fully turbulent flow ($x/c = 0.7$), the output signal remains high, but the deviations above and below the mean become more consistent. From these type signals obtained over a series of test conditions, the extent of laminar flow could be determined. Figure 10 shows the measured upper surface transition location on the NLF(1)-0414F airfoil with lift coefficient for constant R_c's. The results confirm that the existence of laminar flow was maintained rearward to $x/c = 0.70$ at design $c_\ell = 0.40$ and $R_c = 10 \times 10^6$. The corresponding wake-rake drag measurements (fig. 8) with free transition support the thin-film results. However, as the lift coefficient is increased above design c_ℓ, transition gradually moves forward, and at $c_\ell = 0.50$, $(x/c)_{tr} = 0.50$. The successful verification of this airfoil's performance is attributed to holding very tight surface tolerances during fabrication and obtaining test results in a wind tunnel with good flow quality. The fabricated and measured surface waviness was held to $h/\lambda = 1/3000$ for single waves and is shown in figure 6 ($h/\lambda = 0.00033$ at $\lambda/c = 0.056$) to be well below other data and that allowable for multiple waves at design $R_c = 10 \times 10^6$.

The measured drag variation with lift for different flap deflections from $-10° < \delta_f < 20°$ is summarized in figure 11 at $R_c = 6 \times 10^6$ and $M_\infty = 0.07$. The results indicate that very low drag values can be maintained over a lift coefficient range from $0 < c_\ell < 1.0$. These results were obtained with a simple flap of 0.125c length and offer the potential for long runs of laminar flow over a wide c_ℓ range. Because the NLF(1)-0414F airfoil was shaped (fig. 7) for long regions of accelerated flow necessary to achieve laminarization followed by a rather steep pressure gradient downstream, a laminar separation bubble was anticipated beyond the pressure minimum at low Reynolds numbers. Such bubbles have inherently unstable characteristics that generally cause transition to rapidly move forward with significant lift losses. The existence of a laminar separation bubble on either surface was detected

by comparison of measured and predicted pressure distributions (not shown) and associated drag level increase from lift-drag polars. These comparisons clearly indicated that a laminar bubble which existed aft of $x/c = 0.70$ for $R_c < 3 \times 10^6$ was nonexistent for $R_c > 4 \times 10^6$.

It is well known that a significant reduction in drag can be realized if flow can be kept attached. One method for reducing the drag associated with the presence of a laminar bubble is to force boundary-layer transition to occur ahead of the bubble causing the flow to remain attached (refs. 42-44). This can be accomplished by the use of turbulators (2D-3D trips, spoilers, sound, passive or active blowing and suction, etc.). Of course, one must account for the "device drag" of the turbulator used. Tests were conducted to evaluate the effectiveness of several turbulators on the NLF(1)-0414F airfoil in the LTPT. Figure 12 illustrates the effect of using simple 2D strips of commercial tape placed at $x = 0.68c$ on both upper and lower surfaces of the model to force transition and eliminate separation bubbles ($R_c = 3 \times 10^6$, $M_\infty < 0.2$, and $\delta_f = 0°$). A tape 0.012 inch thick and 0.25 inch wide was used. The results (figure 12) clearly show a measured reduction in drag coefficient of about 0.0010 at $c_\ell = 0.40$ with the turbulator tape. Apparently, only a small amount of induced energy by turbulators is required to force transition and attachment of laminar separation bubbles.

The effectiveness of turbulators strongly depends both on their geometry and location since they function like trips or roughness which scale with local boundary-layer properties. Other turbulator devices (not shown) were tested aside from the tape and found to be effective. For example, small vortex generators of $h/c = 0.25$, and 15° leading-edge sweep with respect to flow direction, were spaced ($\Delta y/h = 8$) along the model span at $x/c = 0.60$ and $x/c = 0.70$. Results from using these devices proved very effective in forcing transition and bubble attachment but produced undesirable drag penalty. Probably the most effective turbulator, in terms of both forcing laminar bubble attachment and reducing wake drag with no apparent device drag, was a spanwise row of holes (ref. 42) ahead of $x/c = 0.70$. The holes of diameter $d = 0.0018$ inches, located 0.25 inches apart, were drilled through from the top to bottom surface. Since the design pressure distribution (figure 7) generated a pressure differential across the upper and lower surfaces, passive suction and blowing occur, providing a method for energizing the boundary layer that was sufficient to be effective in these tests. In summary, such devices and techniques as described above appear very promising and economically feasible for application and control of laminar separation bubble attachment with subsequent drag reduction.

High-Speed Airfoils - Shaping

It is well known that the subsonic cruise speeds of high performance aircraft are limited by the onset of the transonic drag rise and that the use of wing sweepback delays this onset (ref. 22). Another method for increasing the cruise Mach number is through the use of geometric shaping

which delays the drag rise Mach number. The first airfoils developed in the U.S.A. to delay drag rise were the NACA 1-series (ref. 45). These airfoils were designed to delay the Mach numbers at which supersonic flow first develops locally on the airfoil. These airfoils have significantly higher drag-rise Mach numbers than the earlier NACA four-digit series; however, the low-speed high-lift characteristics are much poorer than those of the earlier airfoils. The NACA 6-series airfoils also provided increased critical speeds with improved drag-rise characteristics compared to the four-digit series but also have small degraded low-speed characteristics. Such airfoils or their derivatives have been used on many first generation subsonic jet aircraft.

The first airfoils designed to purposely delay drag rise by improving the supercritical flow over the upper surface were the "peaky" airfoils. These airfoil shapes generate an isentropic recompression of the supersonic flow on the forward airfoil region and provide some delay in drag rise but also have degraded low-speed characteristics compared to the NACA 6-series airfoils. Whitcomb's research efforts (ref. 22) led to designs which allowed the recompression to move far rearward on the airfoil at transonic speeds and resulted in significant delays in drag-rise Mach number without degrading low-speed characteristics.

Based on the encouraging results obtained by geometric shaping to achieve extensive laminar flow on both surfaces of the low-speed NLF(1)-0414F airfoil, effort has been recently directed towards extension of the concepts to higher speed NLF airfoils. Details of the two-dimensional design concepts have been given by Viken (ref. 38) along with wing body integration by Waggoner (ref. 39) and integrated trailing-edge flap design by Morgan (ref. 40). One of the more promising high-speed NLF airfoil concepts has been fabricated and tested in the NASA Langley LTPT and 6x28-inch transonic tunnel (TT) complex to investigate its low-speed high-lift and drag-rise characteristics. This NASA high-speed natural laminar flow airfoil is designated HSNLF(1)-0213. The airfoil was designed for a lift coefficient of 0.25, Mach number of 0.70, chord Reynolds number of $R_c = 10 \times 10^6$, and $t/c = 0.134$. This particular design was for essentially zero sweep.

The HSNLF(1)-0213 airfoil design pressure distribution and section shape are shown in figure 13. Geometric shaping was expected to provide laminar flow rearward to $x/c = 0.55$ on the upper and $x/c = 0.70$ on the lower surfaces up to $R_c < 10 \times 10^6$. In general, the bottom side of the nose was slightly modified from the NLF(1)-0414F to minimize off-design pressure peaks on the lower surface, and upper surface aft camber was reduced to minimize the possibility of turbulent separation.

Results obtained (not shown) from tests in the 6x28-inch TT indicated good agreement between measured and predicted pressure profiles and that drag rise occurred at about $M_\infty = 0.72$ for $c_\ell \approx 0.2$, and design $R_c = 10 \times 10^6$. The level before drag rise, with and without fixed transition at $x/c = 0.05$, was about 20 to 30 percent below that of a good turbulent airfoil. It should be noted that the turbulence and noise levels are believed to be high in the 6x28-inch TT which operates as a

blowdown facility. Thus, poor flow quality contributed to the inability to achieve extensive laminar flow over the model, especially at the higher Reynolds numbers. However, the drag rise characteristics can still be approximated. Surface contour accuracy was measured for the 6-inch chord steel model fabricated and found to be acceptable.

A second HSNLF(1)-0213 airfoil model, fabricated with fiberglass external surfaces, had a 2-foot chord and no flap. This model was tested in the LTPT for low-speed performance evaluation. An example of the results is shown in figure 14 for $M_\infty = 0.168$ and $R_c = 4 \times 10^6$ with and without fixed transition at $x/c = 0.05$. Figure 14 shows that a minimum drag coefficient of about 0.0038 was measured at $c_\ell = 0.2$ or $L/D \approx 53$. The results indicate that the airfoil displayed trailing-edge-type stall characteristics, and a value of $(c_\ell)_{max} \approx 1.55$ was obtained for $R_c = 4 \times 10^6$. It is also apparent that fixing transition had only small effects on the lift performance. Figure 15 shows the effect of Mach number and Reynolds number on the maximum lift performance. While the $(c_\ell)_{max}$ increases with increasing R_c for constant Mach number as expected, there is a small effect of Mach number on the maximum lift. For example, results at $M_\infty = 0.1$ are consistently 0.05 higher than results at $M_\infty = 0.2$ over the Reynolds number range tested. Thus, one cannot simulate Reynolds number effects on $(c_\ell)_{max}$ by increasing Mach number at the same time Reynolds number is increased since they have opposing influences.

Boundary-layer transition locations were also obtained by J. P. Stack (NASA Langley) on both surfaces of the HSNLF(1)-0213 airfoil in the LTPT using surface-mounted thin-film gages. A summary of the transition locations on the upper and lower surfaces compared with predictions from the Eppler theory (refs. 46-47) is shown in figure 16 for $\alpha = 0°$ and chord Reynolds number from 3.0×10^6 to 9×10^6. The data clearly indicate that laminar flow was maintained rearward to about $x/c \approx 0.5$ and $x/c \approx 0.70$ on the upper and lower surface, respectively, up to $R_c = 8 \times 10^6$, before any forward movement of transition was measured.

Low Reynolds Number Airfoils

For airfoils designed to operate at low Reynolds numbers ($R_c < 500 \times 10^3$), the existence of a laminar separation bubble and turbulent separation significantly increase the drag and decrease the lift, both of which contribute to low lift-to-drag ratios. This phenomenon has previously been extensively investigated and discussed (refs. 21, 48-51). Increasing the Reynolds number will reduce the length of the laminar separation bubble and extent of turbulent separation. At positive incidence, the boundary layer, which is laminar along the airfoil's upper-forward surface, separates at the downstream adverse pressure-gradient recovery region. It then quickly undergoes transition to turbulent flow in the separated shear layer.

Depending on the Reynolds number and the severity of the adverse pressure gradient, this separated turbulent boundary layer may or may not reattach to the airfoil surface. If reattachment occurs, the turbulent boundary layer may then separate again near the trailing edge. If the Reynolds number is sufficiently low such that reattachment does not occur, increasing the Reynolds number to some critical value will cause reattachment that corresponds to a dramatic increase in L/D. Thus, the possible existence of both laminar and turbulent separation should be considered in the design and wind tunnel testing of airfoils in the low Reynolds number regime. For example, such airfoils are typical of those on current RPVs, sailplanes, and general aviation aircraft canards.

Mangalam and Pfenninger (ref. 52) have recently designed a low Reynolds number airfoil and tested it in the 12"x18" open-circuit tunnel at the NASA Langley 8-Ft. TPT complex at low speeds. The airfoil section shape and an example of the measured and predicted pressure distributions are shown in figure 17 for $R_c \approx 100 \times 10^3$, $c_\ell = 1.0$, and $\alpha = 4°$. Basically, the airfoil was shaped to have moderate negative camber in the nose region to reduce pressure peaks at off-design and attached flow. The forward lower surface cusp is due to combined leading-edge thickness and camber and requirement for increased mid-chord thickness for structural strength. This airfoil is designated LRN(1)-1007 and represents about a 40% increase in t/c and an appreciable increase in c_ℓ/c_d at design (fig. 18) above previous similar airfoils (ref. 51).

Except for the upper surface aft region, good agreement is shown between the measured and predicted pressures using the Eppler theory (ref. 46) for the smooth model. The measured data indicate a long separation bubble in the rear upper-surface pressure-rise region, with reattachment near the trailing edge. Mangalam and Pfenninger (ref. 52) concluded from these results that at low Reynolds number the laminar boundary layer is highly stable and a number of trips are required in several locations along the chord to promote transition. Applications of the 2-D spanwise trips (ref. 52) eliminated the laminar separation bubble and provided about a 25% increase in lift-drag ratio. Subsequent flow visualization photographs were obtained of the model flow field in the same tunnel, using smoke wire techniques*, and are shown in figure 19 illustrating the occurrence of laminar separation with incidence angle for $R_c = 40{,}000$. Figure 19 shows attached flow over most of the airfoil surface at $\alpha = 3°$. However, for $\alpha = 18°$, separation occurs at the leading edge and never reattaches. Similarly, for $\alpha = -12°$, the lower surface separates without reattachment. It can be seen from these photographs that the measurement and verification of the performance of low Reynolds number airfoils with separated flow become highly questionable.

*Smoke wire technique was developed and results obtained by Amir Bar-Sever and Dr. S. Mangalam, under contract to AAB, NASA Langley.

High-Lift Testing - Sidewall Effects

Depending upon model aspect ratio and facility utilized, testing of airfoils at high angles of attack can result in severe tunnel sidewall interference effects. Large adverse pressure gradients can be induced by the airfoil at incidence that cause the oncoming tunnel sidewall boundary layer to separate, spread downstream and spanwise, and result in a large decrease in airfoil lift. The following results and discussion attempt to illustrate this influence on high-lift performance for low-drag or turbulent airfoils.

Figure 20 shows lift performance results for the same single-element airfoil tested in two different NASA Langley facilities at $M_\infty = 0.30$ and $R_c \approx 6 \times 10^6$. The models tested in the LTPT and 6x28-inch TT had aspect ratios of 1.5 and 1.0, respectively. The results indicate that severe sidewall interference effects occur in the 6x28-inch TT for angles of attack greater than about 10°. This resulted in measured maximum lift coefficient for this airfoil in the 6x28-inch TT that was about 17 percent lower than in the LTPT. Figure 21 shows photographs of oil flow patterns obtained in the 6x28-inch TT with the airfoil having an aspect ratio of 1.0 for $8° < \alpha < 12°$. A complex secondary flow field that nearly dominates the entire model span is seen to develop due to sidewall interference as model incidence is increased. Separated flow occurs on either side of mid-span for $\alpha = 12°$ causing drastic lift loss (fig. 20).

To ensure that models experience uniform, two-dimensional, interference-free air flow when testing multi-element airfoils, some feasible concept is required for tunnel sidewall boundary-layer control (BLC). The LTPT has recently been modified to incorporate a BLC system (ref. 37) which includes both upstream sidewall suction slots ahead of the model and tangential blowing slots located on the same tunnel walls near the model juncture region. This system provides a means for reducing the oncoming boundary-layer thickness as well as energizing the boundary layer locally around the model for maintaining attached flow as incidence is increased.

The effects of sidewall BLC on the lift performance of a multi-element airfoil using tangential slot blowing near the nose and flap regions are shown in figure 22. Slot blowing is applied until the lift at mid-span (obtained from surface pressure data) is approximately matched with the lift near the tunnel sidewalls. The results shown in figure 22 indicate large differences in lift coefficient at high incidence between the mid-span and near wall regions without blowing compared to the results with blowing. With blowing, the measured lift values at mid-span and near wall regions are essentially the same. Thus, one should use caution in conducting high-lift performance testing

or verification to select a facility that accommodates large-aspect-ratio models or that has sidewall control for reducing interference effects to insure meaningful results.

In addition to the interference effects produced by separation of the boundary layer on the vertical sidewalls, corrections are required to account for model and wake blockage and interference due to test section floor and ceiling constraints on streamline curvature. Tests are planned in the LTPT to evaluate these interference effects by testing high-lift models with chord lengths of 1 and 2 feet. Lift coefficients up to about 4.0 are expected from these models.

High-Speed Airfoils - Shaping and Suction

The concept of combining geometric shaping and suction laminarization on airfoils to achieve very low drag dates back to the late 1930's (refs. 4-5). The basic feasibility of achieving full chord laminar flow with very low drag on swept nonsupercritical LFC wings was pioneered by Pfenninger (ref. 5) with suction applied through many closely spaced surface slots on the wings. Results were obtained on large chord wing sections (modified 66012) of 30° sweep and $t/c \approx 0.12$ in three different wind tunnels. These studies confirmed earlier beliefs that results were dependent on the characteristic turbulent and acoustic disturbance levels in each facility. Since this research demonstrated the potential for significant drag reduction through application of LFC, an interest in evaluating the feasibility of combined suction laminarization and supercritical airfoil technology at conditions which are typical of high-performance transports has been generated. Therefore, a large chord ($c = 7.07$ ft.) swept supercritical LFC airfoil with suction slots has been designed, constructed, and recently tested in the NASA Langley 8-Ft. TPT. This NASA airfoil is designated SCLFC(1)-0513F. Details of the airfoil and suction system design along with the test setup have been reported (ref. 19). Requirements for this test also included modification of the wind tunnel to achieve the desired flow quality and test section wall contouring to simulate free air flow about an infinitely yawed model at transonic speeds.

Figure 23 shows the design pressure distribution for the swept supercritical LFC airfoil. Attempts were made to minimize suction laminarization through a highly tailored pressure distribution and choices of leading-edge sweep, chord Reynolds number, and crossflow Reynolds number (ref. 6). Depending on geometry, boundary-layer instabilities that can occur on swept wings are leading-edge instability, Tollmien-Schlichting tangential instability, crossflow instability, and Taylor-Goertler instability due to surface concave curvature. These instability regions are shown in figure 23 for the LFC airfoil and indicate where combined shaping and suction were applied for control. A rather large supercritical zone (aspect ratio ≈ 0.37) exists over the upper surface flat-pressure region followed by a steep rear pressure rise. The lower surface is seen to be heavily loaded in the fore and aft regions with a small supercritical zone in between.

Figure 24 shows the measured and designed chordwise pressure distributions for two chord Reynolds numbers at $M_\infty = 0.82$ on the LFC airfoil that are generally in good agreement. Essentially shock-free flow was obtained for the results shown. The slightly overall higher velocities on the upper surface and chordwise deviations from design are attributed to classical problems associated with transonic wind tunnel testing, wall interference, and model deformation under design air loads. The velocity field between the upper surface-tunnel wall channel (supersonic bubble zone) was higher than predicted due to the contoured liner wall and inability to completely account for three-dimensional boundary-layer displacement thickness effects in the design analysis. Measured coordinate deviations from design, obtained with a dial indicator under applied simulated design airloads, were about 0.003-inch on the model forward upper surface at mid-span. This deviation corresponds to $h/\lambda = 0.0015$ for multiple waves and is shown in figure 6 to meet allowable criteria based on earlier results at low speeds but well above the projected goal for supercritical airfoils (ref. 19). The data in figure 24 indicate that flow separation occurs on the lower surface at about $x/c = 0.80$ when the Reynolds number is increased from $R_c = 10 \times 10^6$ to 20×10^6. Since transition correspondingly moved rapidly forward on the lower surface, the flow into the trailing-edge cusp apparently was unable to sustain the adverse pressure gradient. This separated flow changes the local effective area distribution of the test section resulting in a slightly higher freestream Mach number and increased sensitivity to local surface conditions and pressure variations.

The measured chordwise suction coefficient (C_Q) distribution required to maintain full-chord laminar flow over both surfaces at the design Mach number and $R_c = 10 \times 10^6$ is shown in figure 25 compared to prediction. The measured required suction was higher than the theory over most of the upper and lower surfaces. The higher suction requirements were attributed to the previously discussed higher than anticipated velocities and surface pressure irregularities, the higher suction control required to overcome cross-flow instabilities associated with the steep pressure gradients on the upper and lower surface nose and aft regions, and the minimization of centrifugal Taylor-Goertler type boundary-layer instabilities and interactions with crossflow in the concave regions of the lower surfaces.

A summary of the measured transition locations on the LFC airfoil upper surface for several Mach numbers is shown in figure 26. These results were obtained from a grid of flush-mounted surface thin-film gages to detect the state of the local boundary layer. Full chord laminar flow was maintained on both surfaces up to $R_c = 10 \times 10^6$ for all Mach numbers. As Reynolds number was increased for constant Mach number, transition moved gradually forward on the upper surface. The Reynolds number at which this forward movement began was dependent on Mach number. It was concluded that suction laminarization over a large supercritical zone is feasible to high chord Reynolds numbers even under non-ideal surface conditions on a swept LFC airfoil at high-lift conditions.

Analysis of both spanwise pressure distributions and transition patterns revealed that the flow over the yawed wing was not two-dimensional at $M_\infty < 0.80$. It is believed that the resulting spanwise gradients influenced suction requirements and laminarization at the lower speeds.

The total drag at $M_\infty = 0.40$ and 0.82 for $R_c = 10 \times 10^6$ with full chord laminar flow is seen in figure 27 to be equal to about $(c_d)_{tot} = 0.0030$. This represents about 60-percent drag reduction as compared to an equivalent turbulent airfoil drag level of about $c_{dw} = 0.0080$ and a lift-to-drag ratio of about 180 based on design c_ℓ. Total drag is the sum of measured wake rake drag (c_{dw}) at mid-span and the suction drag (c_{d_s}) penalty required to maintain laminar flow. The suction required to maintain full chord LFC was somewhat higher than anticipated (figure 25) and the contribution of suction drag penalty was about 40-percent for the upper and 60-percent for the lower surface. The increase in wake drag for $M_\infty > 0.70$ was attributed to the formation of a weak shock wave at the leading-edge region as the supersonic bubble began to develop. As the bubble develops ($0.78 < M_\infty < 0.80$), full chord laminar flow still exists, but periodic turbulent bursts occur over the upper surface causing an increase in wake drag. As Mach number is increased to 0.82, the supersonic zone spreads rearward to about 80-percent chord, the bursts disappear, and the wake drag returns to near its subsonic level (figure 27). It is concluded that the basic phenomenon of applying suction laminarization over an extensive supercritical zone is feasible up to high chord Reynolds numbers as demonstrated on a swept LFC airfoil at high lift conditions. The major difficulty or influence in achieving this result was that of overcoming the classic "non-ideal" wind tunnel test environment and hardware tolerances.

CONCLUDING REMARKS

Laminarization through passive or active methods is a boundary-layer stability problem which has been proven to be difficult to analyze, control, and verify. This is especially true as one moves from low to high speeds where swept-back wings and higher lift-to-drag ratios are desirable for improved aircraft performance.

In an effort to simulate flight conditions on models in wind tunnels, we need to better understand the environment and its influences on high-lift and low-drag testing. Several factors influencing the performance of low-drag airfoils have been identified which are primarily involved with overcoming the classic "nonideal" wind tunnel test environment and hardware tolerances.

NASA Langley has recently developed several advanced low-drag airfoil concepts with and without boundary-layer suction control for achieving extensive laminar flow with very low drag. Verification of the anticipated performance of these concepts through wind tunnel testing, from subsonic to transonic speeds, has shown significant improvements in

lift-to-drag ratio over previous airfoils designed for low drag. Probably the most significant result at subsonic speeds is that the lift performance for these lower drag airfoil concepts is not degraded with fully turbulent flow over the airfoil surface. This provides a factor of safety in aircraft operation, should laminar flow be lost due to contamination. Suction laminarization over a large supercritical zone has been shown to be feasible to high chord Reynolds numbers even under non-ideal surface conditions on a swept LFC airfoil at high lift.

REFERENCES

1. Jacobs, Eastman N.: "Preliminary Report on Laminar Flow Airfoils Method Adopted for Airfoil and Boundary Layer Investigations", NASA WR L-345, June 1939.

2. Abbot, Ira H.; and von Doehhoff, Albert E.: "Theory of Wing Sections", New York, Dover Publications. 1959.

3. Pfenninger, W.: "Investigations on Reduction of Friction on Wings, in Particular by Means of Boundary Layer Suction." NASA Technical Memorandum 181, August 1947.

4. Lachmann, G. V. (Editor): Boundary Layer and Flow Control, Vol. 2, Pergamon Press, 1961.

5. Pfenninger, W.: Laminar Flow Control, Laminarization. AGARD-R-654, Von Karmon Institute, Belgium, 1977.

6. Pfenninger, W.; Reed, H. L.; and Dagenhart, J. R.: "Design Considerations of Advanced Supercritical Low Drag Suction Airfoils." Viscous Flow Drag Reduction, Vol. 72, Progress in Astronautics and Aeronautics, 1980.

7. Gray, W. E.: "Transition in Flight on a Laminar-Flow Wing of Low Waviness (King Cobra)". R.A.E. Report N. 2364, March 1950.

8. Gray, W. E.; and Fullam, P. W. J.: "Comparison of Flight and Wind Tunnel Measurements of Transition on a Highly Finished Wing (King Cobra)". R.A.E. Report No. 2383, June 1950.

9. Pfenninger, W.; and Growth, E.: "Low Drag Boundary Layer Suction Experiments in Flight on a Wing Glove of an F-94A Airplane with Suction Through a Large Number of Fine Slots". Boundary Layer and Flow Control, Vol. 2, G. V. Lachmann, ed., 1961, pp. 981-999.

10. Fowell, L. R.; and Antonatos, P. P.: "Laminar Flow Control Flight Test Results, Some Results from the X-21A Program". Part 2, Recent Developments in Boundary Layer Research, Part IV, May 1965. AGARDograph 97, pp. 1-76.

11. Loftin, L. K. Jr.; and Burrows, D. L.: "Investigations Relating to the Extension of Laminar Flow by Means of Boundary-Layer Suction Through Slots". NACA TN 1961, 1949.

12. Braslow, A. L.; Burrows, D. L.; Tetervin, N.; and Visconti, F.: "Experimental and Theoretical Studies of Area Suction for the Control of the Laminar Boundary Layer on an NACA 64A010 Airfoil". NACA Rept. 1025, 1951.

13. Holmes, Bruce J.; Obara, Clifford, J.; and Yip, Long P.: "Natural Laminar Flow Experiments on Modern Airplane Surfaces." NASA TP-2256, June 1984.

14. Holmes, Bruce J.; Obara, Clifford J.; Martin, Glenn L.; and Domack, Christopher S.: "Manufacturing Tolerance for Natural Laminar Flow Airplane Surfaces." SAE Paper 850863, April 1985.

15. Croom, C. C.; and Holmes, B. J.: "Flight Evaluation of an Insect Contamination Protection System for Laminar Flow Wings." SAE Paper 850860, April 1985.

16. Somers, Dan M.: "Design and Experimental Results for a Flapped Natural Laminar Flow Airfoil for General Aviation Applications." NASA Technical Paper, 1965.

17. Viken, Jeffrey K.: "Aerodynamic Design Considerations and Theoretical Results for a High Reynolds Number NLF Airfoil." Master's Thesis. George Washington University. January 1983.

18. McGhee, Robert J.; Viken, Jeffrey K.; Pfenninger, W.; Beasley, William D.; and Harvey, William D.: "Experimental Results for a Flapped NLF Airfoil with High Lift/Drag Ratio." NASA TM-85788, May 1984.

19. Harvey, W. D.; and Pride, J. D.: "The NASA Langley Laminar Flow Control Airfoil Experiment." AIAA Paper No. 82-0567, March 1982.

20. Reshotko, Eli: "Control of Boundary Layer Transition." AIAA-85-0562, 1985.

21. Mueller, T. J.: "The Influence of Laminar Separation and Transition on Low Reynolds Number Airfoil Hysteresis." AIAA-84-1617, 1984.

22. Whitcomb, R. T.: "Review of NASA Supercritical Airfoils." ICAS Paper No. 74-10, Aug. 1974.

23. Dagenhart, J. R.: "Amplified Crossflow Disturbances in the Laminar Boundary Layer on Swept Wings with Suction." NASA TP-1902, November 1981.

24. El-Hady, Nabil M.: "HADY-I, a FORTRAN Program for the Compressible Stability Analysis of Three-Dimensional Boundary Layers." NASA CR-3467, 1981.

25. Srokowski, A. J.; and Orszag, S. A.: "Mass Flow Requirements for LFC Wing Design." AIAA Paper No. 77-1222, Aug. 1977.

26. El-Hady, N. M.: "On the Stability of Three-Dimensional Compressible Nonparallel Boundary Layers." AIAA Paper No. 80-1374, July 1980.

27. Mack, L. M.: "On the Stability of the Boundary Layer on a Transonic Swept Wing." AIAA Paper No. 79-0264, Jan. 1979.

28. Carmichael, B. H.: "Surface Waviness Criteria for Swept and Unswept Laminar Suction Wings." NOR-59-438, 1959.

29. Carmichael, B. H.: "Surface Imperfection Experiments on a Swept Laminar Suction Wing." Northrop Rept. BLC-124, NOR-59-454, 1959.

30. Poll, D. I. A.: "Leading Edge Transition on Swept Wings." AGARD CP-224, pp. 21-1-21-11, 1977.

31. Ram, R. B.; Vemuru, C. S.; and Harvey, W. D.: "Hybrid Approach to Steady Transonic Normal Shock-Compressible Laminar Boundary Layer Interactions over Airfoils with Suction." AIAA 85-0522, 1985.

32. Pate, S. R.: "Effects of Wind Tunnel Disturbances on Boundary-Layer Transition with Emphasis on Radiated Noise: A Review." AIAA Paper No. 80-0431, March 1980.

33. Owen, F. K.; Stainback, P. C.; and Harvey, W. D.: "An Evaluation of Factors Affecting the Flow Quality in Wind Tunnels." AGARD Conference Proceedings No. 348 on Wind Tunnels and Testing Techniques, July 1979.

34. Harvey, W. D.; and Bobbitt, P. J.: "Some Anomalies Between Wind Tunnel and Flight Transition Results." AIAA Paper 81-1225, 1981.

35. Harvey, W. D.; Stainback, P. C.; and Owen, F. K.: "An Evaluation and Assessment of Flow Quality in Selected NASA Wind Tunnels." NASA TM-85659, August 1983.

36. Stainback, P. Calvin; and Owen, F. Kevin: "Dynamic Flow Quality Measurements in the Langley Low Turbulence Pressure Tunnel." AIAA-84-0621, 1984.

37. McGhee, Robert J.; Beasley, William D.; and Foster, Jean M.: "Recent Modifications and Calibration of the Langley Low-Turbulence Pressure Tunnel." NASA TP-2328, July 1984.

38. Viken, J. K.: "Boundary Layer Stability and Airfoil Design." NASA CP-2413, 1986.

39. Waggoner, E. G.: "Computational Wing Design Studies Relating to Natural Laminar Flow." NASA CP-2413, 1986.

40. Morgan, Harry L.: "High-Lift Flaps for Natural Laminar Flow Airfoils." NASA CP-2413, 1986.

41. Dagenhart, J. Ray; and Stack, John P.: "Boundary-Layer Transition Detection Using Flush-Mounted Hot-Film Gages and Semiconductor Dynamic Pressure Transducers." AIAA Paper No. 82-0593, March 1982.

42. Horstmann, K. H.; and Quast, A.: "Reduction of Section Drag by Blowing Through Rows of Holes in Areas of Laminar Separation Bubbles," Technical Soaring, Vol. VII, No. 1, September 1981.

43. Pfenninger, W.: "Investigation on Reductions of Friction on Wings in Particular by Means of of Boundary Layer Suction. NACA TM 1181, August 1947. (Translated from the German "Untersuchungen uber Reibungsverminderungen an Tragflugeln, insbesondere mit Hilfe von Grenzschtabsaugung," Mitteilungen aus dem Inst. fur Aerodynamik, Nr. 13, Zurich, 1946).

44. Champine, R.; and Blanchard, W.: "Airplane Model Experiments with Wedge-Shaped Strips Mounted on the Upper Wing Surface." Soaring, vol. 18-19, 1955.)

45. Stack, John.: "Tests of Airfoils Designed to Delay the Compressibility Bubble. NACA TN-976, 1944.

46. Eppler, Richard; and Somers, Dan M.: "A Computer Program for the Design and Analysis of Low-Speed Airfoils," NASA TM-80210, August 1980.

47. Eppler, Richard; and Somers, Dan M.: "Low Speed Airfoil Design and Analysis." Proceedings of the NASA Advanced Technology Airfoil Research Conference, NASA CP-2045, Part 1, March 1978.

48. Mueller, T. J.; and Pohlen, L. J.: "Boundary Layer Characteristics of the Miley Airfoil at Low Reynolds Numbers," AIAA-83-1795, July 1983.

49. Miley, S. J.: "On the Design of Airfoil for Low Reynolds Numbers," Proceedings of the Second International Symposium on the Technology and Science of Low-Speed Motorless Flight, The Soaring Society of America, Inc., September 1974.

50. Lissaman, P. B. S.: Low Reynolds Number Airfoils. Annual Review of Fluid Mechanics, Vol. 15, 1983.

51. Pfenninger, W.: Experimental Investigation of an Airfoil with High Lift-To-Drag Ratios at Low Reynolds Numbers. Northrop BLC-Report 84 (NAI 560188), 1956.

52. Mangalam, S.; and Pfenninger, W.: "Wind-Tunnel Tests on a High Performance Low-Reynolds Number Airfoil." AIAA-84-0628, 1984.

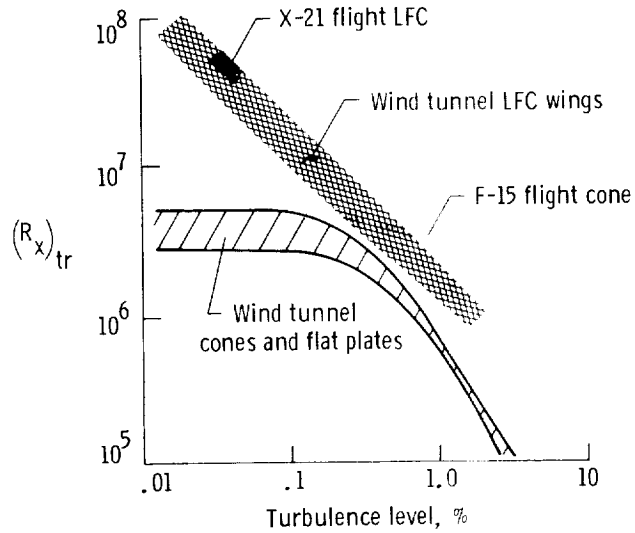

Figure 1.- Influence of turbulence level on transition Reynolds number.

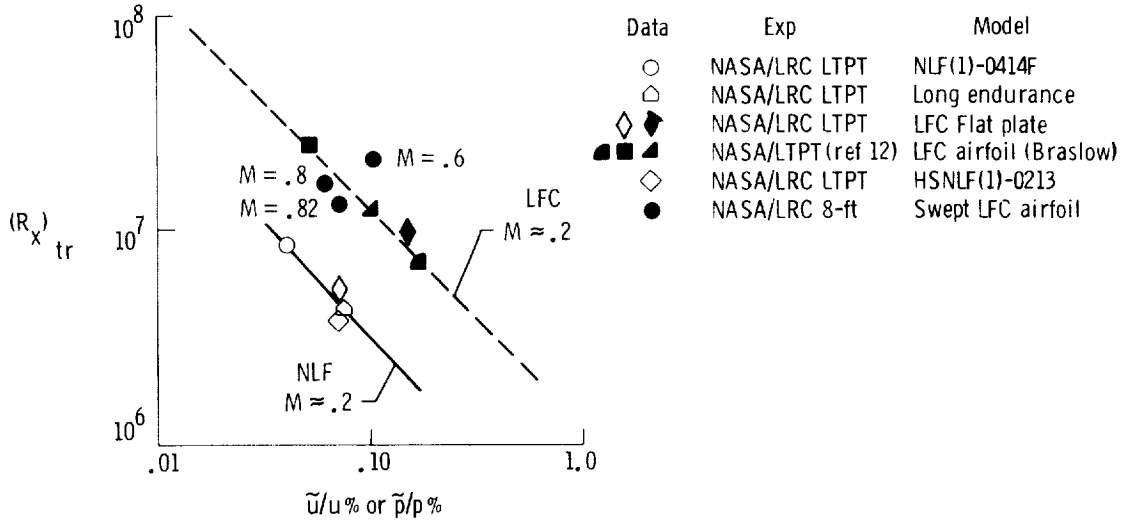

Figure 2.- Influence of tunnel disturbance level on measured maximum transition Reynolds number for low-drag airfoils in two NASA Langley tunnels.

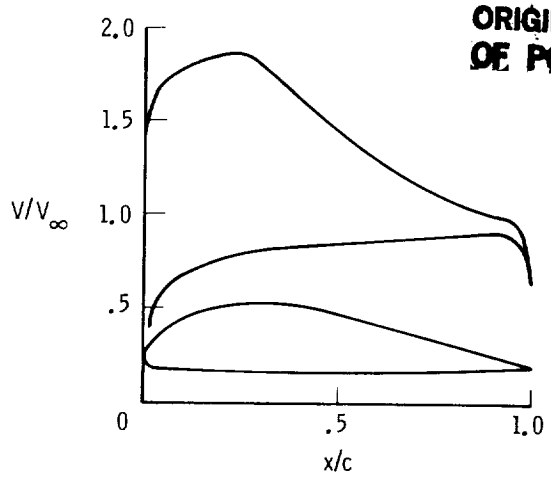

Figure 3.- Velocity distribution for long endurance airfoils.

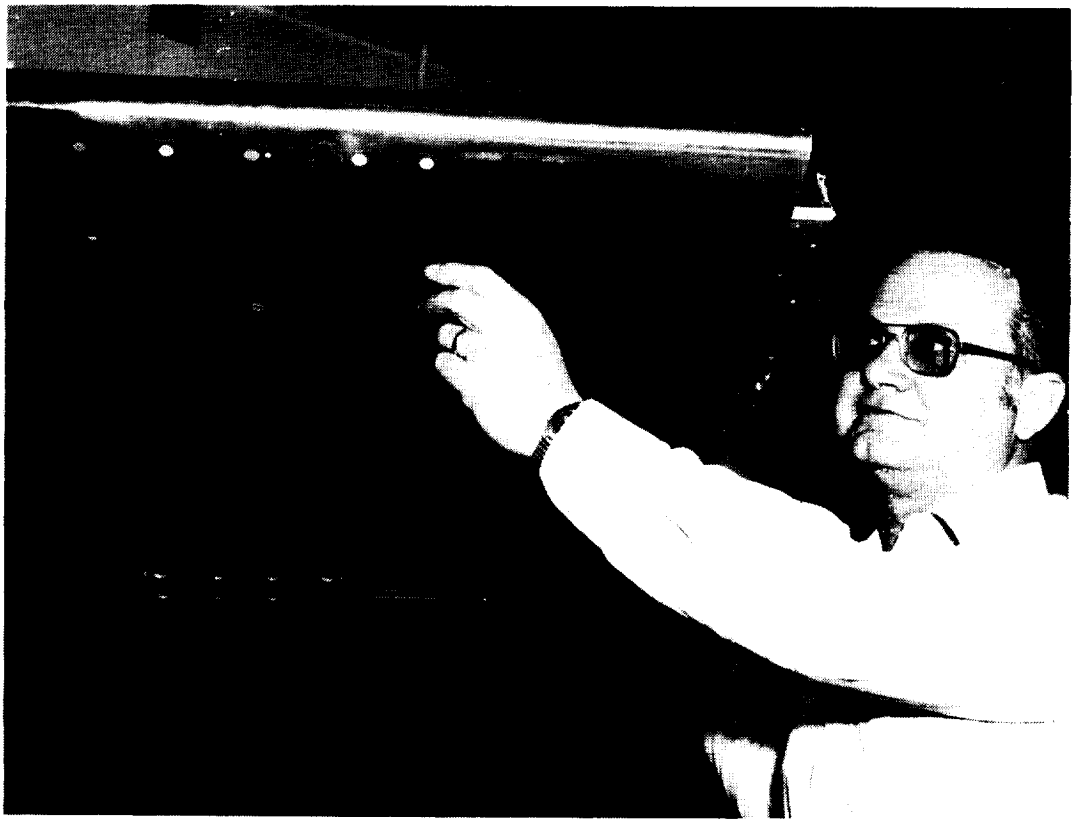

Figure 4.- Long endurance laminar-flow airfoil tested in the Low-Turbulence Pressure Tunnel.

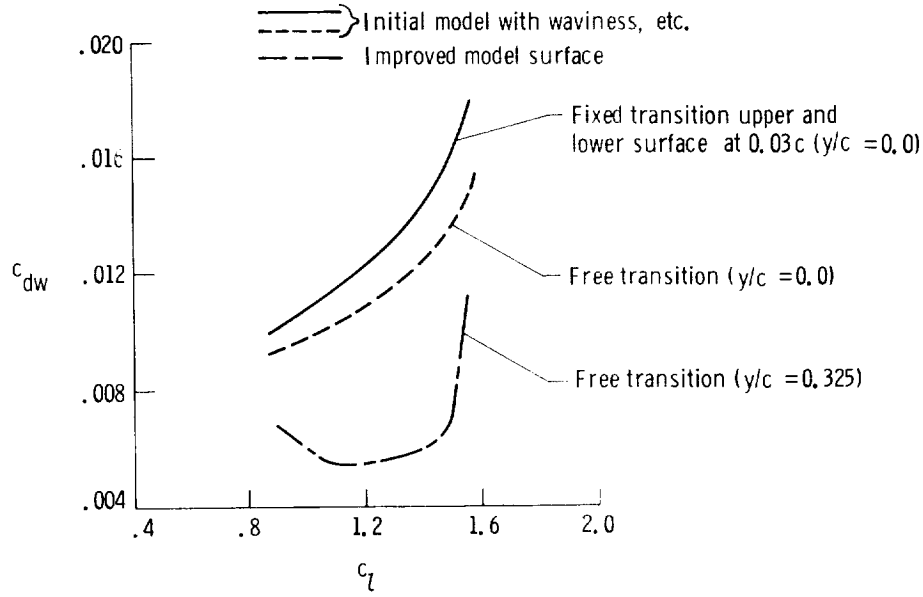

Figure 5.- Long endurance laminar flow airfoil results from LTPT. $M = 0.10$, $R_c = 14 \times 10^6$.

$$\left(\frac{h}{\lambda}\right) \leq \frac{1}{3}\left[\frac{59000 \cos^2 \Lambda}{\lambda/c\,(R_c)^{1.5}}\right]^{.5} \quad ; \Lambda = 30°$$

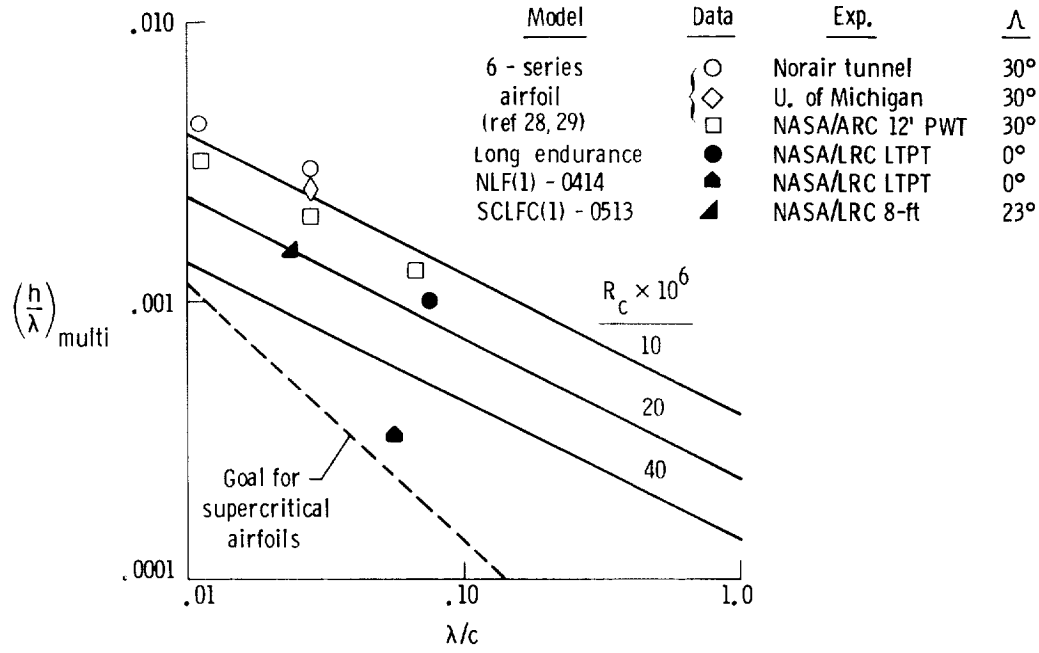

Figure 6.- Permissible amplitude ratio (h/λ) of multiple waves for airfoils in wind tunnels.

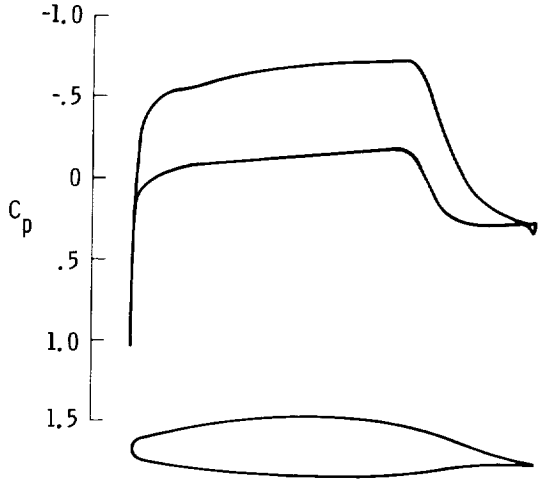

Figure 7.- Calculated pressure distribution for NLF(1)-0414F airfoil at design conditions. c_ℓ = 0.43, M = 0.40; R = 10.0 × 10^6.

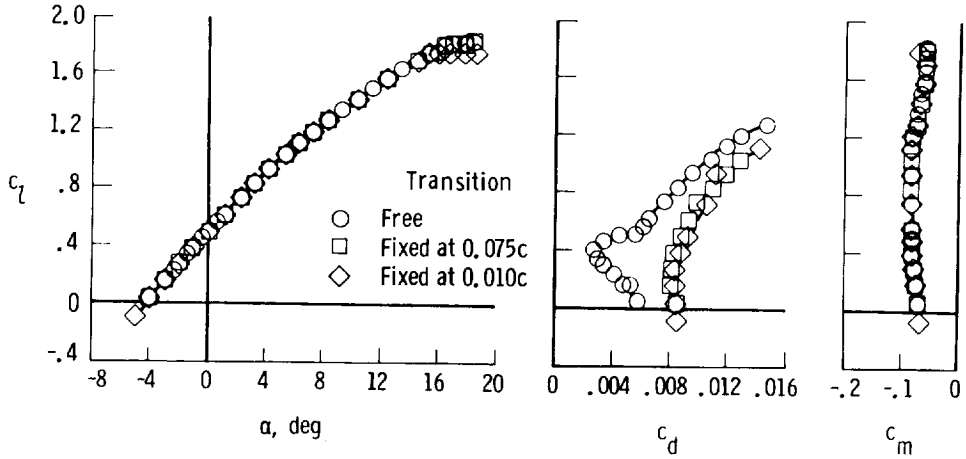

Figure 8.- Section data for NLF(1)-0414F airfoil. R_c = 10 × 10^6, M = 0.10.

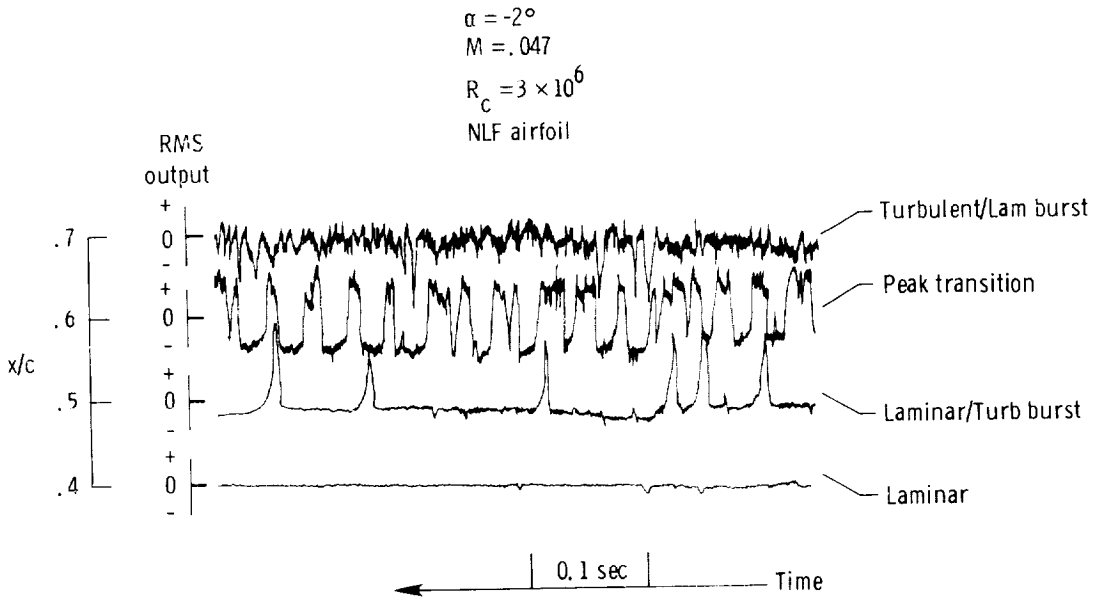

Figure 9.- Example oscillograph recorder traces of thin-film gage RMS output signals with time for state of boundary-layer detection.

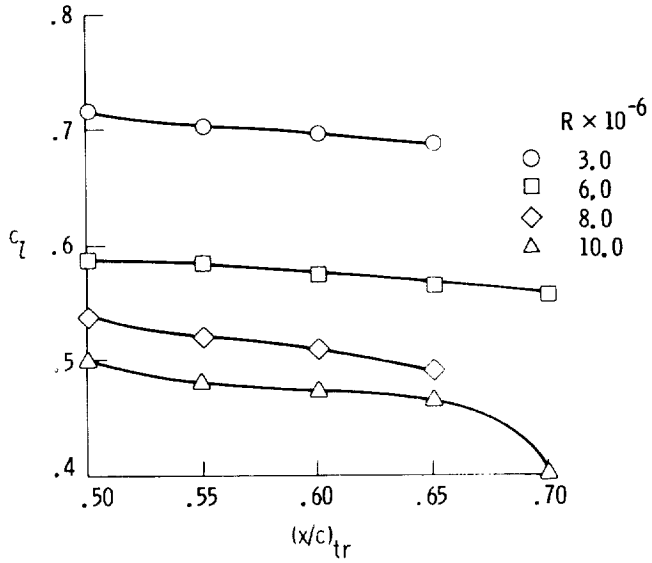

Figure 10.- Upper-surface transition location as determined from thin-film data for NLF(1)-0414F airfoil.

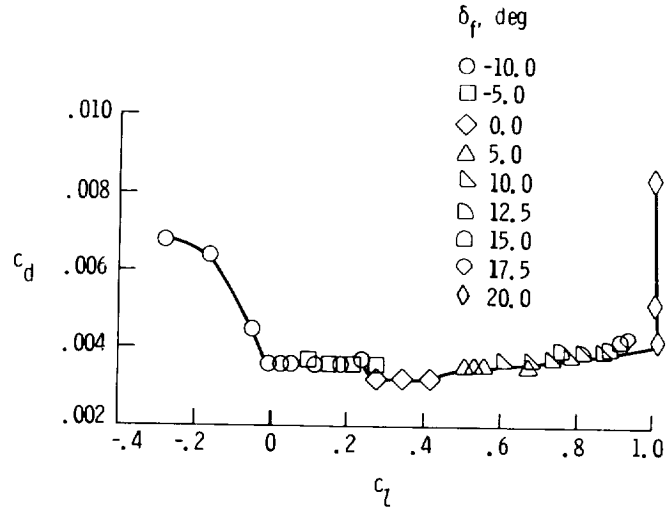

Figure 11.- Effects of flap deflection for NLF(1)-0414F airfoil. $R_c = 6.1 \times 10^6$, $M = 0.07$.

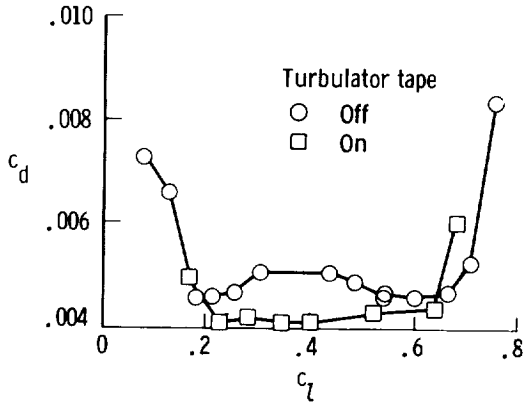

Figure 12.- Effect of turbulator tape on section characteristics for NLF(1)-0414F airfoil. $R_c = 3.0 \times 10^6$; $M \leq 0.20$; $\delta_f = 0°$.

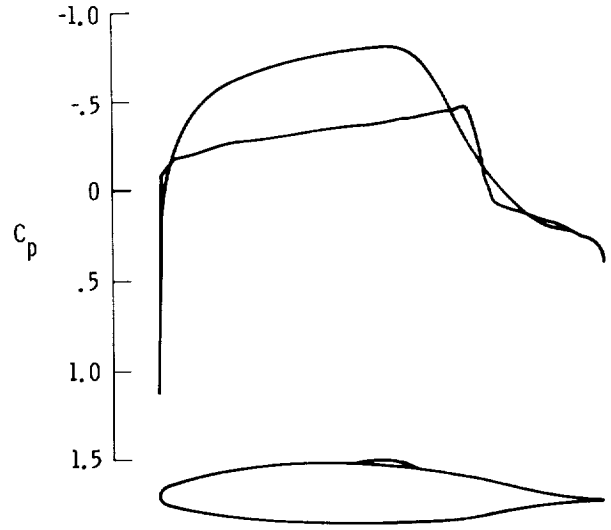

Figure 13.- Design pressure distribution for HSNLF(1)-0213 airfoil. M = 0.70; c_ℓ = 0.20.

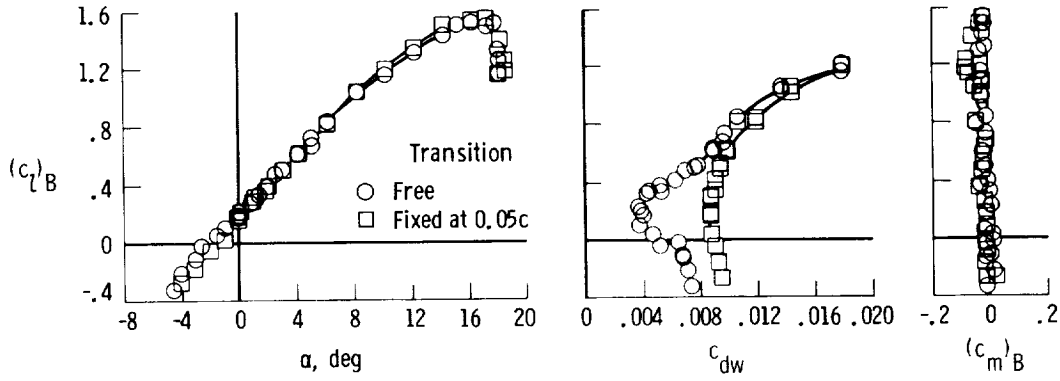

Figure 14.- Section data for HSNLF(1)-0213 airfoil in LTPT. M = 0.168; $R_c = 4 \times 10^6$; $\delta_f = 0°$.

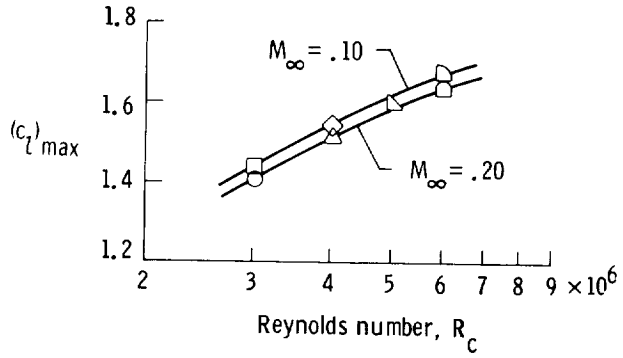

Figure 15.- Effect of Mach number and Reynolds number on maximum lift coefficient performance for NASA HSNLF(1)-0213 airfoil; $\delta_f = 0°$.

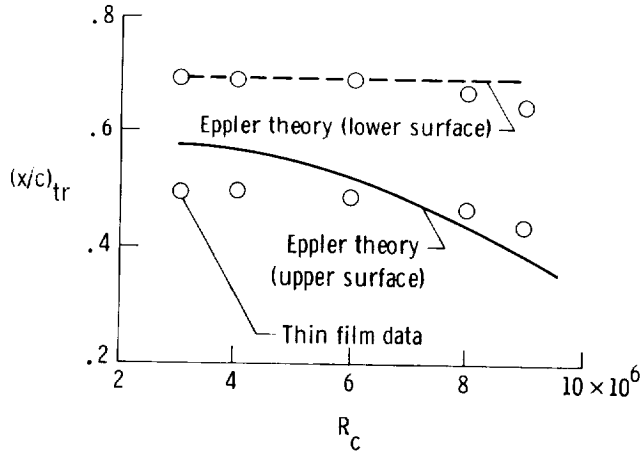

Figure 16.- Transition location for HSNLF(1)-0213 airfoil; $M < 0.20$, $\alpha = 0°$.

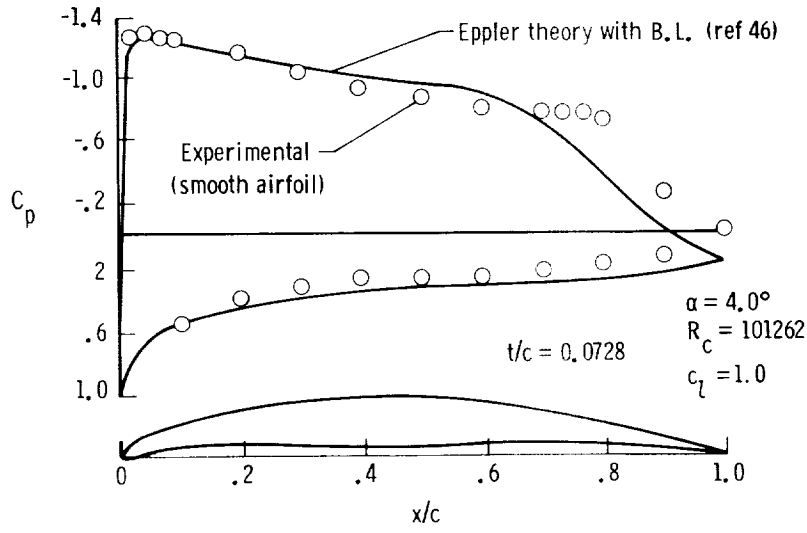

Figure 17.- Measured and predicted pressure distribution for LRN(1)-1007 airfoil.

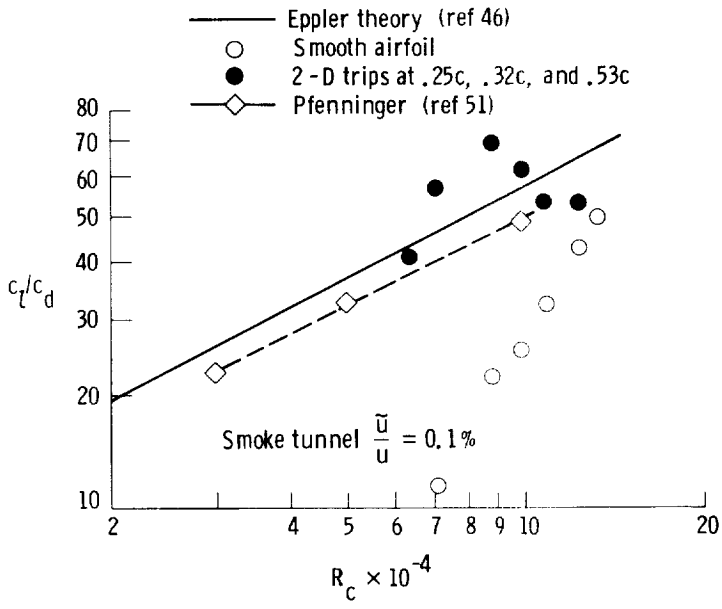

Figure 18.- Maximum lift/drag variation with Reynolds number on LRN(1)-1007 airfoil.

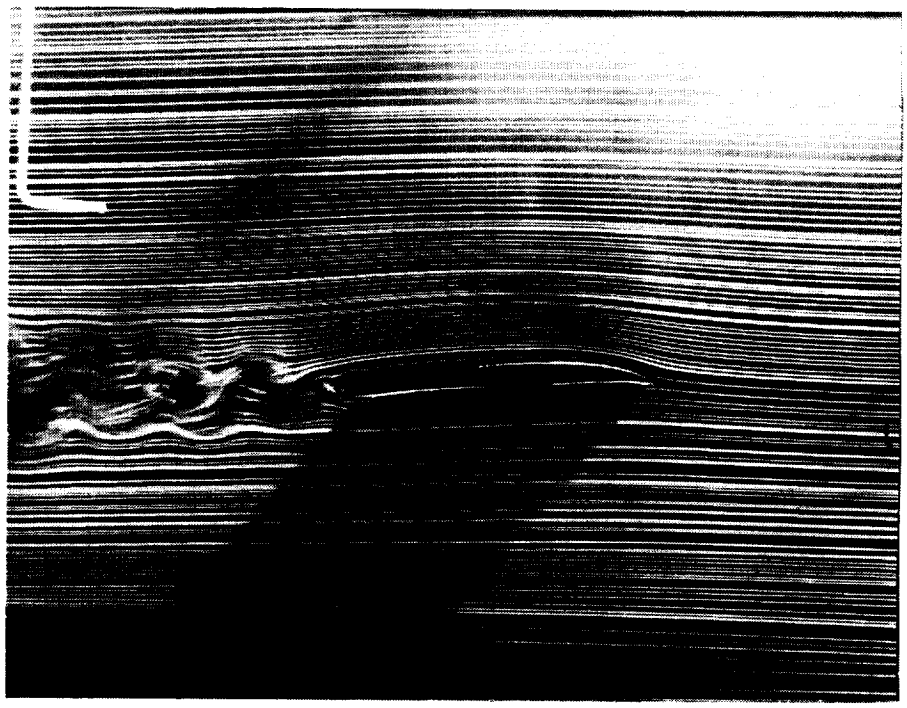

(a) α = 3°.

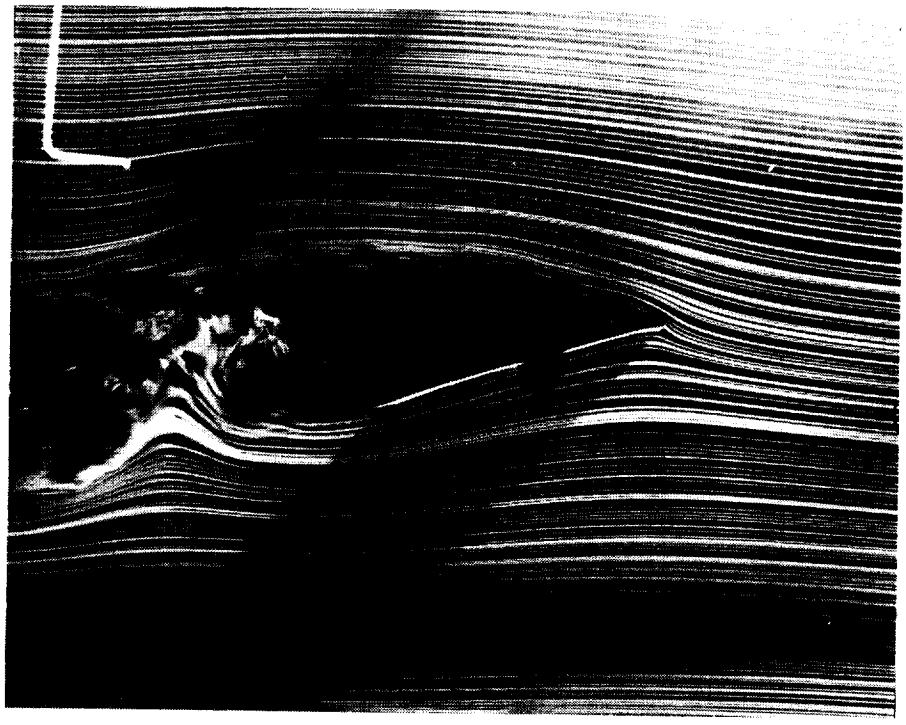

(b) α = 18°.

Figure 19.- Smoke-wire flow visualization photographs for LRN(1)-1007 airfoil. R_c = 40,000.

(c) $\alpha = -12°$.

Figure 19.- Concluded.

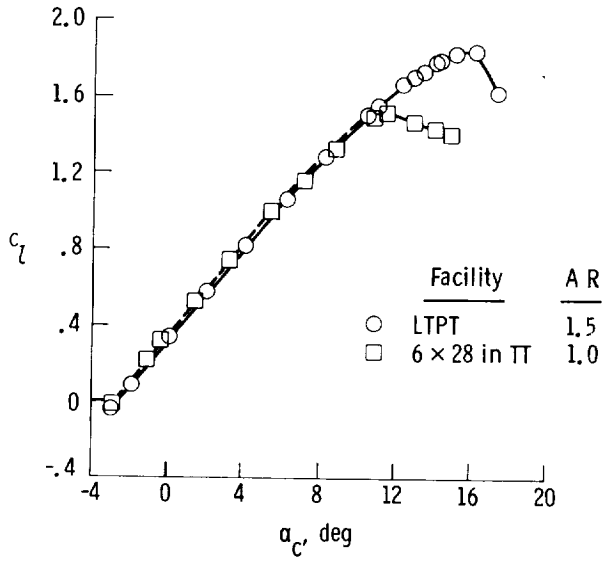

Figure 20.- Tunnel sidewall effects for single-element airfoil. $M \approx 0.30$; $R_c \approx 6.0 \times 10^6$.

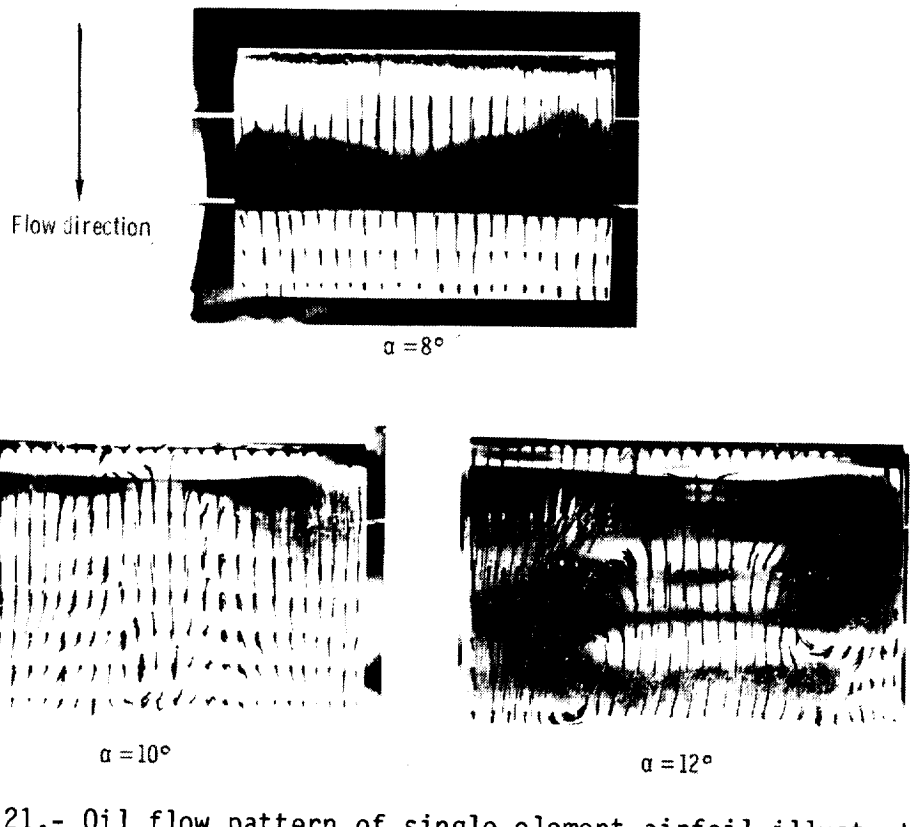

Figure 21.- Oil flow pattern of single-element airfoil illustrating tunnel sidewall effects in 6 × 28-inch TT.

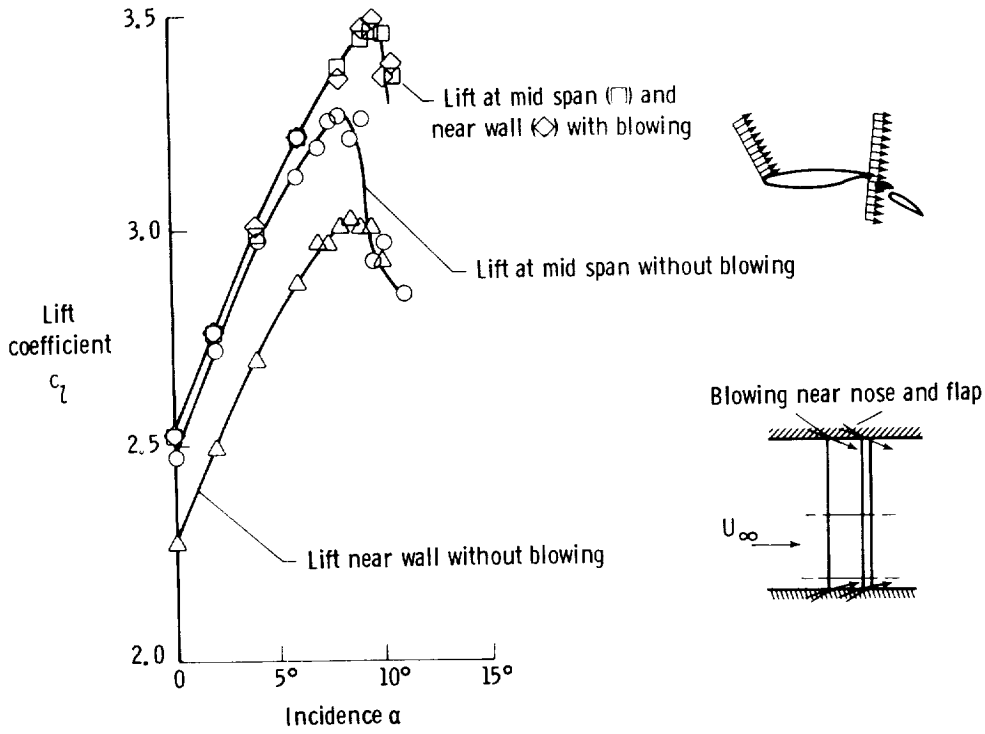

Figure 22.- Typical tunnel sidewall effects for multi-element airfoil showing requirement for sidewall boundary-layer control.

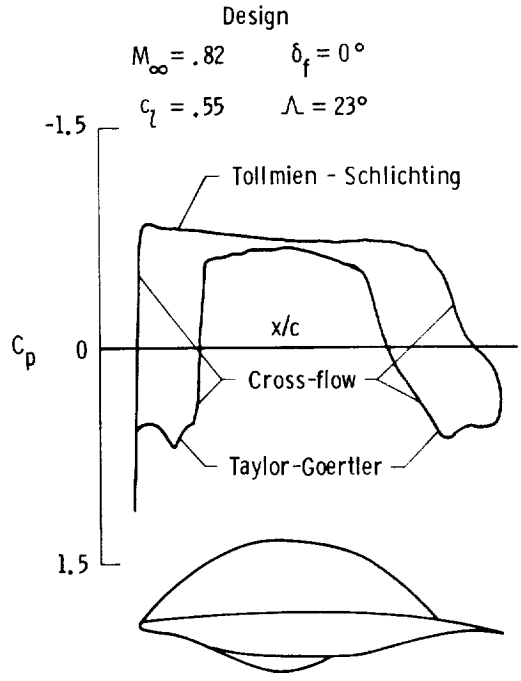

Figure 23.- Design chordwise pressure distributions and sonic lines on the LFC airfoil section.

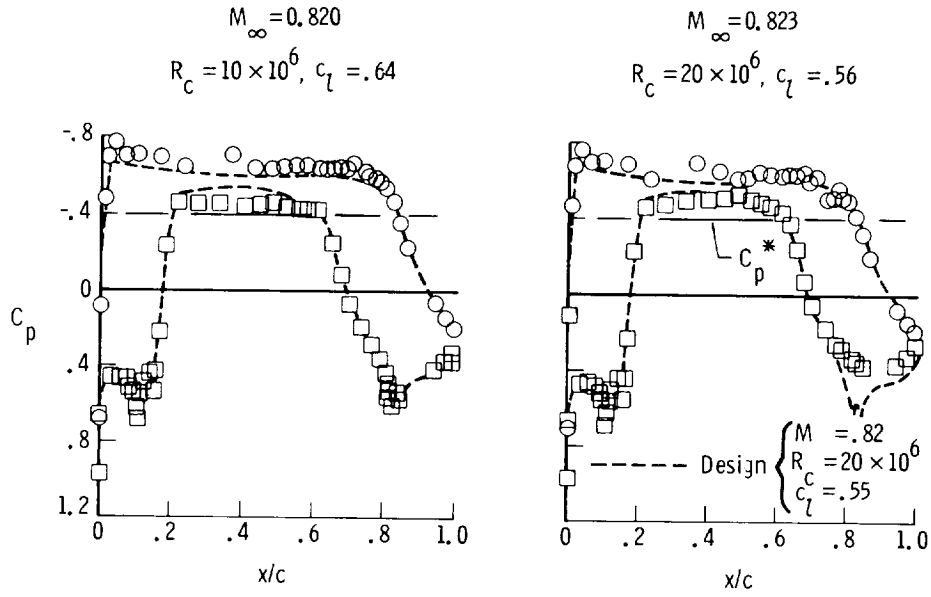

Figure 24.- Comparison of measured and design pressure distribution for swept LFC airfoils.

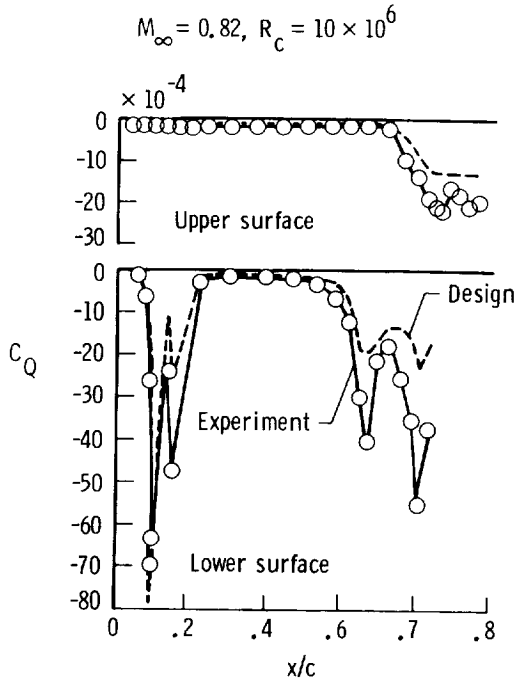

Figure 25.- Measured and design suction distributions for swept LFC airfoil.

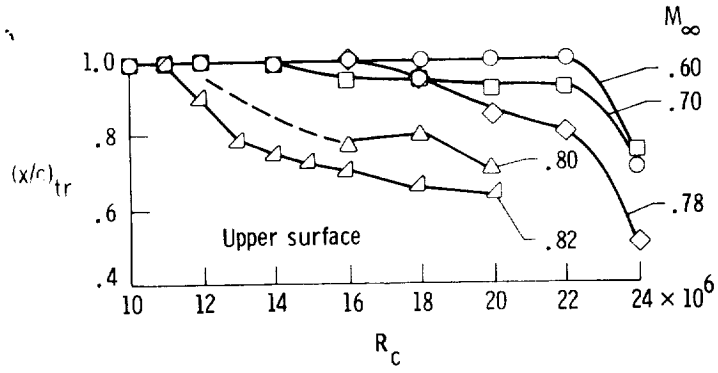

Figure 26.- Variation of measured transition location with Reynolds number for swept LFC airfoil.

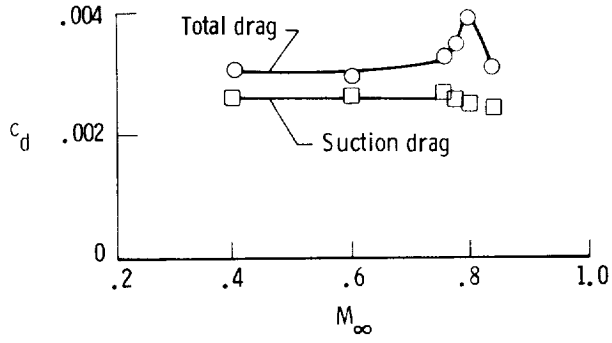

Figure 27.- Measured variation of drag with Mach number for swept LFC wing. $R_c = 10 \times 10^6$.